Detecting the Impact of Climate Change on Land Cover and Land Surface Temperature in Baghdad by Using Remote Sensing.

Elaf Amer Alyasiri, Department of Geography, College of Education and Human Sciences, University of Babylon, Hillah, Iraq.
Email: Ealyasiri@uobabylon.edu.iq | ORCID: 0000-0001-8002-4683

Abstract: in this presented search study, the impact of Climate Changes (CC)global warming on land cover Change (LCC) and Land Surface Temperature (LST) in Baghdad was mapped and analyzed for the years 2013 and 2023. Landsat 8 data for the mentioned years were used as input data. Water, vegetation, and impervious surface indices were applied to map Land Cover Change (LCC), and land surface temperature was used to map the urban heat temperature of Baghdad. The outcome result presented, there was an increase in the water index from 1.3% in 2013 to 1.8% in 2023. Vegetation index had a negative outcome. Approximately 42% of the study area in 2013 had decreased to 35.6% in 2023. Impervious surface index (ISI) had increased over the Land Cover (LC) and indicates that the percentage of impervious surface coverage increased from 56.6% in 2013 to 62.5% in 2023. Land Surface Temperature (LST) was measured for the mentioned years as well to see the impact of Climate Change (CC), the Land Surface Temperature (LST) maps present the highest for 2013 was 32.87 C^o and the lowest was 21.35 C^o. For 2023 the height temperature was recorded 31.15 C^o and the lowest 22.88 C^o. Comparing the Land Surface Temperature (LST) with NASA power data skin surface temperature founding, for April 2013 the skin surface temperature was recorded as the highest 37.03 C^o and the lowest was 9.96 C^{o,} and the data for April 2022 the highest 36.12 C^o and the lowest was recorded as 12.32 C^o.

***Key Words**: Land Surface Temperature (LST), NDVI, NDISI, NDWI, Climate Change.*

رصد تأثير التغير المناخي على الغطاء الأرضي ودرجة حرارة سطح الأرض في محافظة بغداد باستخدام الاستشعار عن بعد

م.د. إيلاف عامر الياسري، قسم الجغرافيا، كلية التربية للعلوم الإنسانية، جامعة بابل، الحلة، العراق.
Email: Ealyasiri@uobabylon.edu.iq | ORCID: 0000-0001-8002-4683

الملخص: في هذا البحث تم رسم وتحليل خرائط الغطاء الأرضي ودرجة حرارة سطح الأرض في محافظة بغداد للسنة 2013 و2023 لرصد التغير المناخي. استخدمت بيانات لاندسات 8 للسنوات المذكورة أعلاه لشهر نيسان لاستخراج مؤشرات المياه والغطاء النباتي والاسطح ذات الانعكاسية العالية (المنطقة الحضرية والتربة الجرداء) ومن ثم استخراج درجة حرارة سطح الأرض في بغداد. أظهرت النتائج أن هناك زيادة في مؤشر المياه لعام 2013 بحوالي 1.3% من عام 2023 1.8%. كما أن مؤشر الغطاء النباتي نتائجه سلبية حيث سجل ما يعادل 42 % في عام 2013 وقد وانخفض إلى 35.6 % في عام 2023. وقد زادت مساحة مؤشرات الاسطح ذات الانعكاسية العالية على الغطاء الأرضي، حيث ان نسبة التغطية المساحية للغطاء ذات الانعكاسية العالية ارتفعت من 56.6% في عام 2013 إلى 62.5% في عام 2023. اظهرت خرائط درجة حرارة سطح الأرض ان درجة الحرارة العظمى لعام 2013 كان 32.87 درجة مئوية الصغرى كانت 21.35 درجة مئوية وفي عام 2023 كانت درجة الحرارة العظمى 31.15 درجة مئوية والصغرى 22.88 درجة مئوية. مقارنة درجة حرارة سطح الأرض مع بيانات وكالة ناسا لدرجة حرارة سطح الأرض لشهر نيسان 2013، سجلت درجة حرارة سطح الارض العظمى 37.03 درجة مئوية والصغرى 9.96 درجة مئوية، وبيانات شهر نيسان 2022 حيث سجلت العظمى 36.12 درجة مئوية والصغرى 12.32 درجة مئوية.

1. Introduction

Land Surface Temperature (LST) is a critical factor for studying the impact of Climate Change (CC) on the Earth's physical and chemical factors. It contains the effects of atmosphere and ground to interact between the surface and the atmosphere. The most crucial issue facing the globe, especially in urban areas, is the increase in surface temperature caused by transforming vegetated areas into impermeable areas, as well as the conversion of wetlands and vegetated areas into agricultural land or barren wastelands. These changes affect the amount of solar radiation absorbed, surface temperature, heat transfer to the soil, and the near surface atmosphere (Mallick et al., 2008). It also impacts on energy and water balance and effect on environmental processes (Oke & Cleugh, 1987; Pal & Ziaul, 2017).

The swift expansion of urban areas leads to a significant loss of vegetation cover, increasing LST in these cities (Yang et al., 2017).Indeed, the growth in population and increasing number of cities have a significant impact on the environment. Thus, urbanization is directly linked to many environmental issues and is one of the primary factors contributing to CC. As the population grows and demands various facilities such as housing, industries, roads, and other infrastructure, it leads to significant changes in LC within a specific region (Sun et al., 2017). Over the last 20 years, there have been notable changes in Land Cover (LC) patterns due to ongoing urbanization (Khandelwal et al., 2018). These changes have led to increases in LST in cities, where the average temperature is 2-5°C higher than in nearby villages or districts. These thermal islands have negative impacts on urban hydrology and the environment. Detecting changes in LC, spatial mapping is one of the key tools for identifying spatial and temporal changes in an area (Ullah et al., 2019; Khandelwal et al., 2018).

According to estimates by the United Nations, LST will rise with other types of pollution, putting 69% of the world's population at risk of exposure by 2050. The global human population reached about 8.0 billion in 2022 and is likely to increase about 2 billion people in the next 30 years, which it is currently 8 billion and expected to be 9.7 billion in 2050. It could rich at nearly 10.4 billion in the mid of 2080s. (United Nations, 2024). The change on environmental and associated impacts, driven by Land Cover Changes (LCC) are increasingly becoming global problems. (K. Li et al., 2020a; Qin & Karnieli, 1999; Rasul et al., 2018).

In recent decades, multispectral imagery, various remote sensing data, and GIS techniques have become widely available as sources for a better understanding of the various elements of the Earth's environment, mapping LC and calculating LST (Hart & Sailor, 2009; Zha et al., 2003; Al Rakib et al., n.d.; Zhang et al., 2017; Avdan & Jovanovska, 2016). The main goal of this study is to detect the impact of the environmental change on LST and LC in Baghdad. This article examines the temperature characteristics throughout selected periods (2013 and 2023) in various types of LC, including vegetation, water, and impervious surface area.

2. Related research

Since the 1960s, researchers have been using remotely sensed data and GIS techniques to analyze CCCC's impact on LST and LC. The research on LST dynamics has significantly improved computing methods using remote sensing data and multiple sensors.Nichol & To (2012) examined the LST and stress in Hong Kong. Neteler (2010) calculated the LST of the alpine environment in the Alps mountains. Ogashawara et al. (2012) Studied the correlation between urban growth, water bodies, vegetation density, and LST in Brazilian cities. Lee et al. (2012) used Landsat and Aster data to measure the LST intensity of Phoenix and Arizona. Gallo & Tarpley (1996) Link between LST and Normalized Difference Vegetation Index (NDVI). Vegetation areas can reduce LST or have a cooling influence on the ambient temperature. Chen et al. (2006) A The normalized difference bareness index (NDBI) was developed to differentiate between bare land and other land use classes using Landsat data. However, it was found that built-up areas showed higher NDBI values than bare land, making this index unsuitable for use in urban areas in semiarid environments. H. Li et al. (2017) NDBI and unsupervised classification was used to map bare soil area by using Landsat images. Z. Zhang et al. (2008) NDBI are often used with high accuracy in humid regions, but there is a need for improved indices for bare soil in dry areas.. Xu (2010) Proposed a Normalized Difference Impervious Surface Index (NDISI) for estimating impervious surfaces, and it was demonstrated that NDISI can efficiently extract impervious surfaces. Xu (2010) proposed NDISI for estimating impervious surfaces by applying Landsat imageries on Fuzhou City and the Aster imageries on Xiamen City in China. Powell et al. (2008) extracted the impervious surfaces in the Snohomish area of Washington by using spectral and spatial resolution data based on classifying impervious surfaces and bare soil. Streutker (2002) Studied the characteristics of LST in terms of magnitude and spatial extent without using in situ measurements to determine if there is a correlation between heat island magnitude and rural temperature. Voogt & Oke (2003) Thermal remote sensing has been used over urban areas to assess the LST, to perform LC classifications, and as input for models of the climate of urban areas. K. Li et al. (2020b) reported an effect on the global environment, climate change, and environmental development. Edan et al. (2021) analyzed the predicted land use LCC and their effects on the seasonal variations in LST in Al Kut, Iraq during the summer and winter seasons. they were utilizing Landsat TM/OLI images from the years 2000, 2010, and 2020 to assess the historical LC and LST status using remote sensing techniques. Al-Hameedi et al. (2022) had chosen a range of natural and human induced factors as risk parameters. Specifically, changes in LC and land LST are considered important factors that have led to large scale change of environment.

3. Materials and Methods

3.1 Study Site

Baghdad is the capital of the Republic of Iraq, covering a total area of 5170 square kilometers and comprising 32 administrative units. It is situated in the central part of Iraq, located between longitude 44° 24′ and 44° 40′ E and latitude 33° 19′ and 33° 32′ N. Baghdad is bordered by the Diyala province to the East, Wasit, and Babil provinces to the South, Anbar province to the West, and Salah al-Din province to the North see Figure 1. The estimated total population of Baghdad is 8,126,755. The city has a dry and warm climate, with intense summer temperatures sometimes exceeding fifty degrees Celsius and dry atmospheric conditions. Baghdad is also prone to severe dust storms, which scientists attribute to global warming and Iraq's desert climate (Central Bureau of Statistics Iraq, 2018).

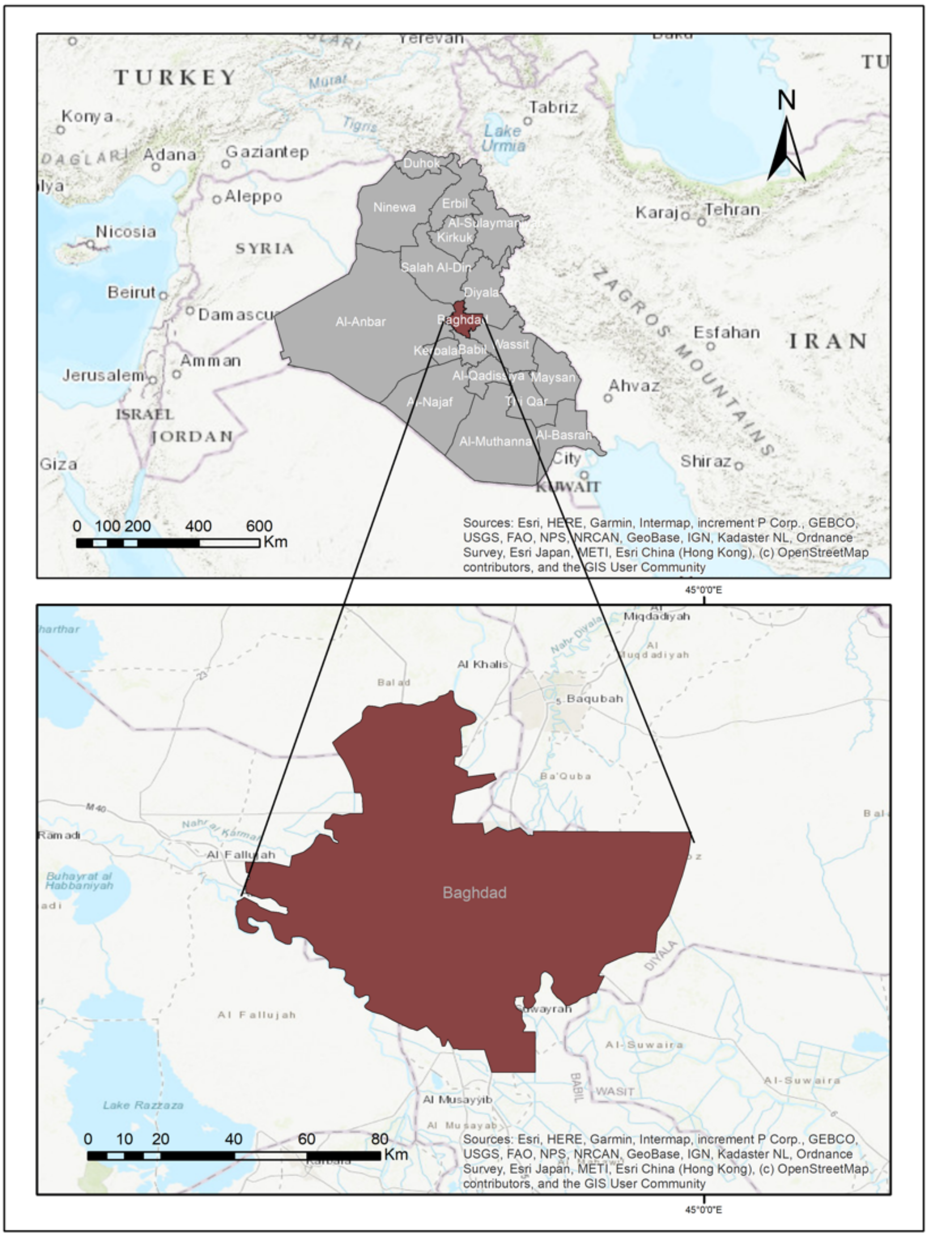

Figure 1. Baghdad's Location of Iraq.

3.2 Data

The spectral reflectance arc illustrates the connection between the electromagnetic spectrum and the percentage of reflectance for a particular material. LC and LST were assessed across the study area for 10 years, from 2013 to 2023. This analysis utilized data sets from Landsat-8 LC and LST, which were acquired from the United States Geological Survey (USGS) Satellite datasets were taken on (2/4/2013 at 07:38:37 and 17/4/2023 at 07:33:09) (EarthExplorer, 2024). Datasets that used were projected to the Universal Transverse Mercator (UTM), with map projection system zone 38N, and datum of World Geodetic System 84 (WGS84). The study utilized thermal observations from Landsat 8. Thermal Infrared Sensors (TIRs) from Landsat 8(band 10) were initially captured at 100 m spatial resolution and later resampled to 30 m, refer to Table 1 for specific details. To maintain consistency, only cloud-free data sets obtained during the Winter season (April) for each year were considered due to the strong seasonality of the study area.

Bands' Number	Wavelength (micrometers)	Resolution (meters)
Band 1 - Coastal aerosol	0.43 - 0.45	30m
Band 2 – Blue	0.45 - 0.51	30m
Band 3 - Green	0.53 - 0.59	30m
Band 4 - Red	0.64 - 0.67	30m
Band 5 - Near Infrared (NIR)	0.85 - 0.88	30m
Band 6 - Shortwave Infrared (SWIR) 1	1.57 - 1.65	30m
Band 7 - Shortwave Infrared (SWIR) 2	2.11 - 2.29	30m
Band 8 – Panchromatic	0.50 – 0.68	15m
Band 9 - Cirrus	1.36 - 1.38	30m
Band 10 - Thermal Infrared (TIRS) 1	10.6 - 11.19	100m (resampled to 30)
Band 11 - Thermal Infrared (TIRS) 2	11.50 - 12.51	100m (resampled to 30)

Table. 1 Landsat 8 Bands Operational Land Imager and Thermal Infrared Sensor.

3 .3 Method

In this research study, the relationship between LST and LC was examined within Baghdad to understand the environmental consequences of climate change. LC was classified into three classes: vegetation, water, and improvised surface, using indices methods. Then, we estimated LST for the city for two periods of time (2013-2023) to examine the relationship between the changes in LC and LST.

3.3.1 Indices

a. Normalized Difference Vegetation Index (NDVI) is the most widely used vegetation index for observing greenery worldwide. Healthy vegetation effectively absorbs the electromagnetic spectrum in the visible range. Chlorophyll is found in plants absorbs the Blue (0.4 - 0.5 µm) and Red (0.6 - 0.7 µm) spectrum and reflects the Green (0.5 – 0.6 µm) spectrum. Healthy plants also exhibit high reflectance in the Near Infrared (NIR) range between 0.7 to 1.3 µm, primarily due to the internal structure of plant leaves. The high reflectance in NIR and high absorption in the red spectrum are used to calculate NDVI. The NDVI formula uses these reflectance values to calculate the index.

NDVI=(NIR–Red) / (NIR+Red) ………………………….…Eq (1)

NDVI= (Band5- Band4) / (Band5+Band4)

Where the red band is (0.64 – 0.67 µm) reflectance and the near-infrared band is (0.85–0.88 µm) reflectance (Table 1). (Crippen, 1990)

b. Normalized Difference Water Index (NDWI) is used to identify and extract water bodies. It is effective because water reflects light differently from land in the visible portion of the electromagnetic spectrum. Liquid water typically reflects more light in the blue spectrum (0.4 - 0.5 µm) than in the green (0.5 - 0.6 µm) and red (0.6 – 0.7 µm) spectra. Clearwater reflects the lightest in the blue region. Additionally, water does not reflect light in the near-infrared (NIR) and beyond. NDWI is calculated using near-infrared (NIR) and short-wave infrared (SWIR) bands, and can be calculated using the following formula**:**

NDWI=(NIR– SWIR) / (NIR+ SWIR) ……………………..Eq (2)
NDWI = (Band 5 – Band 6) / (Band 5 + Band 6)
Where the near-infrared NIR band is (0.85–0.88 µm) reflectance and the Short-Wave infrared (SWIR) is (1.566 – 1.651µm) reflectance (Table 1). (Alyasiri Elaf Amer, 2021; Gao, 1996).

c. Normalized Difference Impervious Surface Index (NDISI) is refers to human-made features that prevent water from penetrating the ground, such as building roofs, asphalt/cement roads, parking lots, sidewalks, and transportation infrastructure. IS serves as an indicator of urbanization and is also crucial for monitoring environmental issues in developed areas, such as the urban heat island effect. Detecting IS in urban areas is vital for understanding their impact. Differentiating between IS and other LC-like instructed material, sand, and bare soil in dry weather areas is challenging due to similar spectral signature values. Built-up areas, bare soil, and sand exhibit spectral response features like IS, causing noise in previous studies. Impervious materials have high emittance in the thermal band (TIR), low reflectance in the near-infrared (NIR) band, and stronger reflectance in the middle infrared.
NDISI = (SWIR -NIR) / (SWIR - NIR) …………………..…… Eq (3)
NDWI = (Band 6 – Band 5) / (Band 6 + Band 5)
Where Short-Wave infrared (SWIR) is (1.566 – 1.651µm) reflectance and near-infrared NIR band is (0.85–0.88 µm) reflectance (Table 1).

3.3.2. Land Surface Temperature

LST is a dynamic quantity that is depend on wavelength. It represents the thermodynamic temperature of the layer that touch the surface of the ground. For ground-based, airborne, and bare soil, LST is the aggregated radiometric surface temperature based on a measure of radiance (Norman & Becker, 1995a). Using data acquired from the thermal infrared sensor (TIRS), Band 11 has significant uncertainty. It is recommended to use TIRS Band 10 data as a single spectral band for LST estimation (Rongali et al., 2018). The following steps were followed to generate LST from thermal bands:

Step 1: conversion of the digital number (DN) of the thermal band to Top of the Atmosphere (TOA) radiance ($L\lambda$). For Landsat 8, band 10 is considered to extract Spectral Radiance (SR) Satellite sensors measure reflectance from the earth's surface as digital numbers (DN) representing every pixel of the image (Yeneneh et al., 2022).

$L\lambda = ML * Q_{CAL} + AL - O_i$ ....Eq (4)

Were is
$L\lambda$ = Spectral Radiance of Top the atmosphere (TOA)
ML= the band specific multiplicative rescal factor Radiance multiplicative (Watts/m2*sr* µm) which is (0.0003342) (Table 2)
QCAL = Digital number (DN) of band 10
AL = the band-specific additive rescaling factor (0.1) (Table 2)
O_i = Correction value for band 10 is 0.29. (Table 2)

Rescaling Factor	Degree	Data Source
M_L (Radiance multi band)	0.0003342	Metadata
A_L (Radiance add band)	0.1	Metadata
K1 (Thermal constant)	774.8853	Metadata
K2 (Thermal constant)	1321.078	Metadata
Oi (Correction value)	0.29	Metadata

Table. 2 Rascal Factors for Landsat 8 (band 10).

Step 2: After the Digital Numbers (DN) would be converted to reflection, the TIRS band would be converted as well from spectral radiance to brightness temperature (BT) by using the thermal constants provided in the metadata file, which is calculated by using the following equation (Avdan & Jovanovska, 2016):

Kelvin (K) to Fahrenheit (°F) Degrees $BT = K2/ \text{In} (K1/L\lambda+1) - 255.372$ …….………Eq (5)
For obtaining the results in Celsius, the radiant temperature is revised by adding the absolute zero (approx. −255.372°F)
Where
BT = is Top of atmosphere brightness temperature (C)
$L\lambda$ = is TOA spectral radiance (W/ (m^2*sr*μm).
K1 = is constant Band (1321.08) (Table 2)
K2 = is constant Band (777.89) (Table 2)
λ = spectral radiance in watts per meter squared steradian micron (W/ (m^2*sr*μm).

Step 3: NDVI: which is calculated by using the following equation:
NDVI = (NIR−RED)/(NIR + RED).…….……………………….. Eq (6)
NDVI= (Band5- Band4)/(Band5+band4)

Where
RED = is DN values of the Red band.
NIR = is DN values of the Near-Infrared band.

Step 4: Proportion of Vegetation (PV) is the vegetation cover and spatial variation of the temperature of the land surface. PV is calculated by following the equation (Sobrino et al., 2004)
$PV= ((NDVI-NDVI_{min})/(NDVI_{max} – NDVI_{min}))^2$ ……………….Eq (7)

Where
PV = Proportion of Vegetation
NDIV= is DN values of NDVI
$NDVI_{min}$= is minimum DN values of NDVI images
$NDVI_{max}$= is maximum DN values of NDVI images.

Step 5: Land Surface Emissivity (E) must be known to estimate (LST), it is acquired by taking the ratio of two different emitted radiances which are the actual emitted radiance and radiance from absolutely emitting surface under the same temperature order (Norman & Becker, 1995b) agricultural areas. (*Climate Adaption Key to Iraq's Stability and Economic Development | United States Institute of Peace*, n.d.)

Desertification and lack of water are caused by river flow fluctuations rendering Iraq vulnerable to the adverse effects of climate change (Sheik Mujabar, 2019;.Avdan & Jovanovska, 2016)

Land Surface Emissivity (E) = 0.004*PV + 0.986

Where
E= is land surface emissivity
PV= is Proportion of Vegetation
0.986 = is corresponds to a correction value of the equation.

Step 6: Estimating LST using the following equation proposed by (Artis & Carnahan, 1982; Yeneneh et al., 2022).

LST= BT/(1+ (Lλ *BT/ C2) * In(E)) ……………………..…..…. Eq (8)

where,
LST = is land Surface Temperature;
BT = is Top of the atmosphere at brightness temperature (^oC)
Lλ = is wavelength of emitted radiance in meters
E = is land Surface Emissivity.
C2 = is h $*$ c/s = 1.4388 $*$ 10^{-2} Mk) = 14388 km
h = is Planck's Constant = 6.626*10^{-34} JS
S = is Boltzmann constant = 1.38*10^{-23} JK
C = is Velocity of Light, and 2.998 *10^8 m/s

4. Results

In the presented research, the spatial relationship between LCC and LST will be examined to map the impact of climate change in Baghdad. Different index methods were used as environmental change indicators. Figure 2 is an index of water bodies in Baghdad for the years 2013 and 2023, which maps the main river (Tigris) and some other water bodies. Table 3 shows the area of the classified LCC for the two selected years (2013, 2023). The NDWI LC in 2013 covered about 1.3% of the area and had increased to 1.8% in 2023.

Year	**2013**		**2023**	
Area	**Km2**	**Percentage**	**Km2**	**Percentage**
NDWI	64	1.3	93	1.8
NDVI	2176	42	1843	35.6
NDISI	2930	56.6	3234	62.5
Sum	5170		5170	

Table 3 Indices Area of Baghdad for the Years 2013 and 2023.

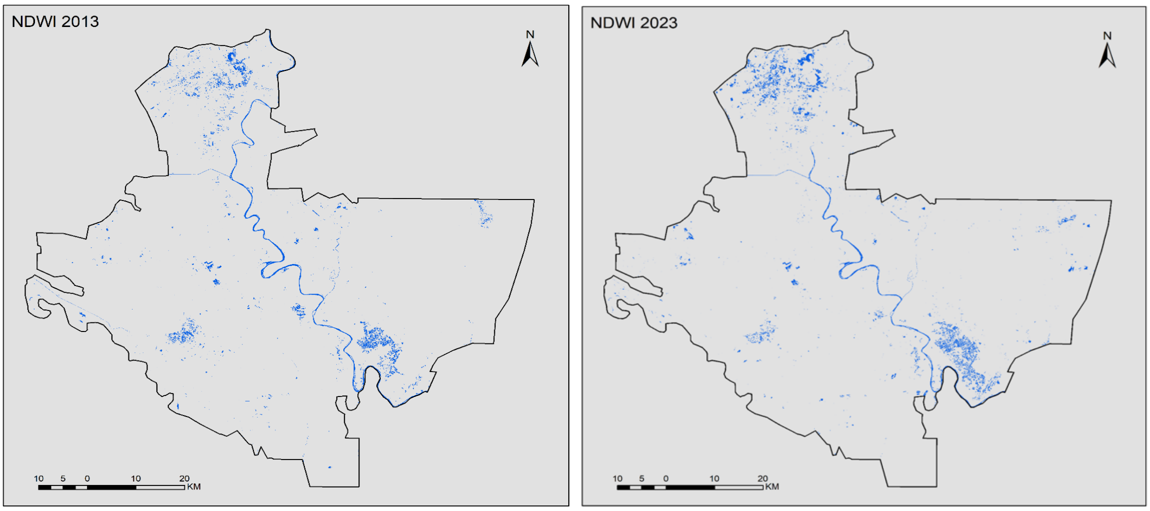

Figure .2 Normalized Difference Water Index of Baghdad for the years 2013 and 2023.

Figure 3 presents the vegetation index for the region around Baghdad for the years 2013 and 2023. As shown in Table 3, the NDVI covered approximately 42% of the study area in 2013. However, by 2023, this coverage had decreased to 35.6%. This decline in vegetation indicates the impact of climate change and urban sprawl.

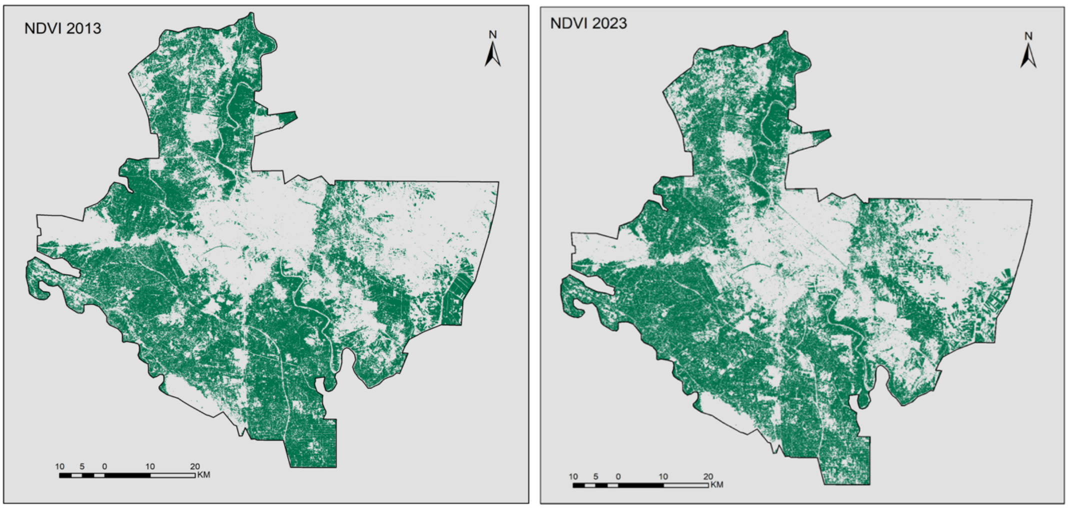

Figure .3 Normalized Difference Vegetation Index of Baghdad for the years 2013 and 2023.

The NDSI of the study area for the years 2013 and 2023 is shown in Table 4. It indicates that the percentage of IS increased from 56.6% in 2013 to 62.5% in 2023. This rise in IS cover over vegetation suggests urbanization growth and a reduction in green areas.

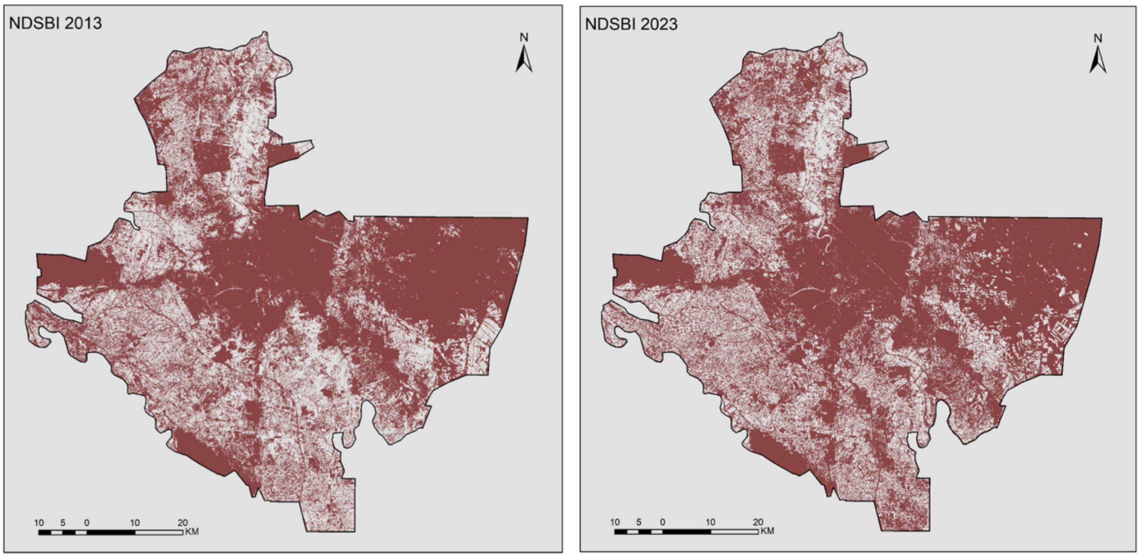

Figure .4 Normalized Difference Impervious Surface Index of Baghdad for the years 2013 and 2023.

Figure 5 presents an urban heat island by using LST for the two years which are 2013 and 2023 of Baghdad. As seen in Figure 4, the temperature of the study area for 2013 ranged between 91.18 ^{o}F 32.87 ^{o}C as the highest and 70.43 ^{o}F 21.35 ^{o}C as the lowest and for 2023 the heights were 88.08 ^{o}F 31.15 ^{o}C and the lowest 73.18 ^{o}F 22.88 ^{o}C.
Comparing the LST temperature to NASA power data and looking at skin surface temperature founding, for April 2013 the skin surface temperature was recorded as the highest 37.03 ^{o}C and the lowest was 9.96 ^{o}C and the data for 2023 was not available, therefore the available data for April 2022 was used to compare the Baghdad land temperature and it was recorded as the highest 36.12 ^{o}C and the lowest was recorded as 12.32 ^{o}C (Nasa Power Ceres, 2024)

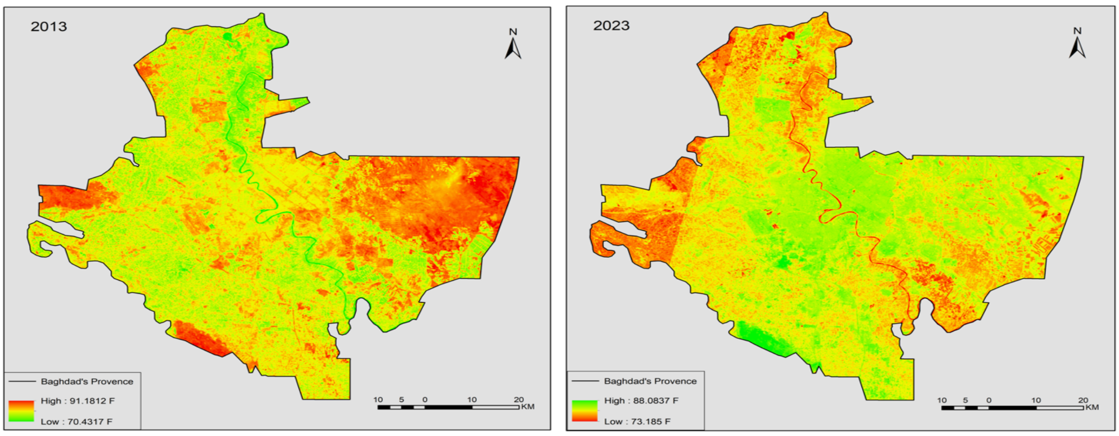

Figure .5 Land Surfers Temperature of Baghdad in Fahrenheit for the years 2013 and 2023.

5. Discussion

The global climate change has been shifting rapidly and the impact of LCC has increased fourfold in the last four decades. Figure 6 shows that the LC in Baghdad has been changing quickly, with urbanized areas and bare soil replacing vegetation. This is contributing to the urban heat island effect and CC. According to the United States Institute of Peace, Iraq is expected to be among the five countries most severely affected by climate change. Figure 5 and Table 3 indicate that LC has increased from 1.3% to 1.8% between 2013 and 2023, as shown in the water index. However, this does not explain the reasons behind this increase. Iraq is already facing a declining water supply and increasing desertification, resulting in the loss of up to 60,000 acres of arable land each year, according to the Iraqi government and United Nations sources. Urbanization has been expanding, with developed surfaces encroaching on vegetation areas, as indicated in Table 3 This aligns with the findings of the report. The impact of CC is increasing each year, while the population of is Iraq is projected to reach 80 million by 2050, while the country's resources are diminishing and facing an issues . The temperatures in Iraq are rising approximately seven times faster than the global average, leading to decreased water levels due to evaporation. By the end of the century, water levels in Iraq are expected to decrease by 30 to 70 percent. This will require long-term planning for resource management, especially in agricultural areas. Noticing in Figure 5 LST of urban areas has risen compared to other LCs. Expanding urbanized areas will intensify the effects of CC and increase concerns about urban heat. Therefore, planners and the government need to acknowledge and address these impacts.

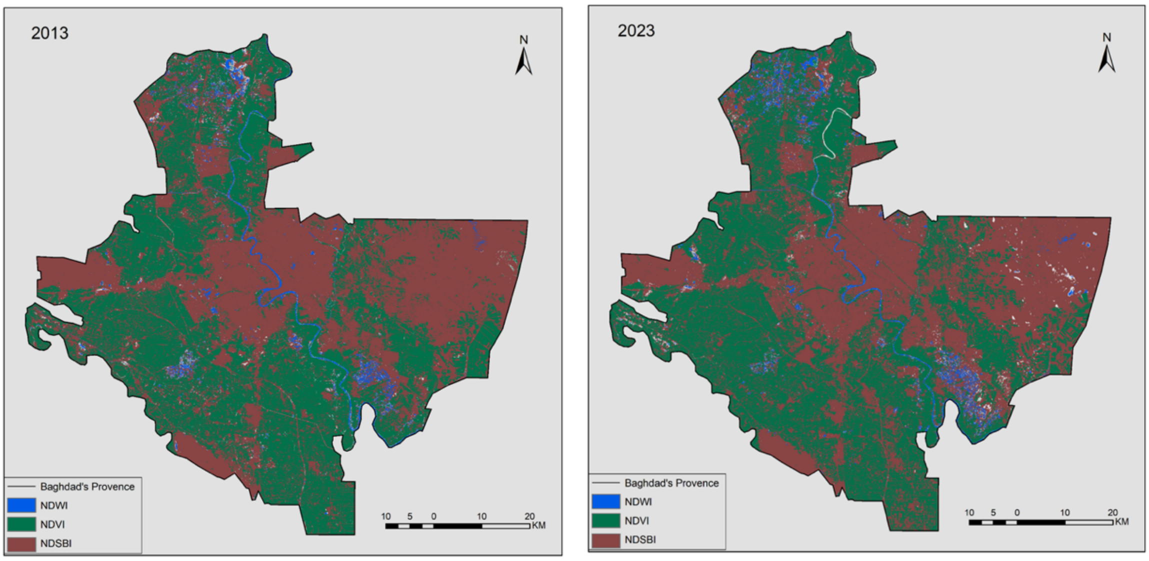

Figure. 6 Land Cover Indices of Baghdad for the Years 2013 and 2023.

6. Conclusion

In conclusion, the study utilized a remote sensing application to examine the effects of climate change on Land Cover (LC) and Land Surface Temperature (LST) in Baghdad. Landsat 8 data from 2013 and 2023 were used to indicate the impact of climate change on mentioned city. Various indices were used such as water, vegetation, and impervious surfaces were employed to map LC, while LST to indicate the urban heat temperature in Baghdad. The results were then compared with NASA power data to confirm the outcome. The study shows an increase in WI, from 1.3% in 2013 to 1.8% in 2023. Conversely, VI experienced a decline, dropping from around 42% in 2013 to 35.6% in 2023. IS exhibited an upward trend, with impervious surface coverage rising from 56.6% in 2013 to 62.5% in 2023. Additionally, urban heat was measured, revealing a peak LST of 32.87°C in 2013 and a low of 21.35°C. The highest recorded temperature for 2023 was 31.15 ^{o}C, while the lowest was 22.88 ^{o}C based on the NASA power data skin surface temperature maps. In April 2013, the highest skin surface temperature was 37.03 ^{o}C, and the lowest was 9.96 ^{o}C. Unfortunately, data for 2023 was not available, so the April 2022 data was used instead to compare Baghdad's land temperatures. This showed the highest temperature as 36.12 ^{o}C and the lowest as 12.32 ^{o}C .

Reference

Al-Hameedi, W. M. M., Chen, J., Faichia, C., Nath, B., Al-Shaibah, B., & Al-Aizari, A. (2022). Geospatial Analysis of Land Use/Cover Change and Land Surface Temperature for Landscape Risk Pattern Change Evaluation of Baghdad City, Iraq, Using CA–Markov and ANN Models. *Sustainability 2022, Vol. 14, Page 8568*, *14*(14), 8568. https://doi.org/10.3390/SU14148568

Alyasiri Elaf Amer. (2021). *Remote Sensing Applications in Population Estimation, Regression Analysis, and Urban Growth Simulation Modeling for a Middle Eastern City - ProQuest*. Northern Illinois University. https://www.proquest.com/openview/bf2618fdd21e0a764aa671b894346310/1?pq-origsite=gscholar&cbl=18750&diss=y

Artis, D. A., & Carnahan, W. H. (1982). Survey of emissivity variability in thermography of urban areas. *Remote Sensing of Environment*, *12*(4), 313–329. https://doi.org/10.1016/0034-4257(82)90043-8

Avdan, U., & Jovanovska, G. (2016). Algorithm for automated mapping of land surface temperature using LANDSAT 8 satellite data. *Journal of Sensors*, *2016*. https://doi.org/10.1155/2016/1480307

Central Bureau of Statistics Iraq. (2018). 2018. https://cosit.gov.iq/ar/?option=com_content&view=article&layout=edit&id=1205

Chen, X. L., Zhao, H. M., Li, P. X., & Yin, Z. Y. (2006). Remote sensing image-based analysis of the relationship between urban heat island and land use/cover changes. *Remote Sensing of Environment*, *104*(2), 133–146. https://doi.org/10.1016/J.RSE.2005.11.016

Climate Adaption Key to Iraq's Stability and Economic Development | United States Institute of Peace. (n.d.). Retrieved May 25, 2024, from https://www.usip.org/publications/2023/11/climate-adaption-key-iraqs-stability-and-economic-development#

Crippen, R. E. (1990). Calculating the vegetation index faster. *Remote Sensing of Environment*, *34*(1), 71–73. https://doi.org/10.1016/0034-4257(90)90085-Z

EarthExplorer. (2024). Retrieved May 21, 2024, from https://earthexplorer.usgs.gov/

Edan, M. H., Maarouf, R. M., & Hasson, J. (2021). Predicting the impacts of land use/land cover change on land surface temperature using remote sensing approach in Al Kut, Iraq. *Physics and Chemistry of the Earth, Parts A/B/C*, *123*, 103012. https://doi.org/10.1016/J.PCE.2021.103012

Gallo, K. P., & Tarpley, J. D. (1996). The comparison of vegetation index and surface temperature composites for urban heat-island analysis. *International Journal of Remote Sensing*, *17*(15), 3071–3076. https://doi.org/10.1080/01431169608949128

Gao, B. C. (1996). NDWI—A normalized difference water index for remote sensing of vegetation liquid water from space. *Remote Sensing of Environment*, *58*(3), 257–266. https://doi.org/10.1016/S0034-4257(96)00067-3

Hart, M. A., & Sailor, D. J. (2009). Quantifying the influence of land-use and surface characteristics on spatial variability in the urban heat island. *Theoretical and Applied Climatology*, *95*(3–4), 397–406. https://doi.org/10.1007/S00704-008-0017-5/METRICS

Khandelwal, S., Goyal, R., Kaul, N., & Mathew, A. (2018). Assessment of land surface temperature variation due to change in elevation of the area surrounding Jaipur, India. *The Egyptian Journal of Remote Sensing and Space Science*, *21*(1), 87–94. https://doi.org/10.1016/J.EJRS.2017.01.005

Kshetri, T. B. (n.d.). *Volume II Geomatics for Sustainable Development NDVI, NDBI, AND NDWI CALCULATION USING LANDSAT 7 AND 8*. Retrieved May 22, 2024, from https://www.researchgate.net/publication/327971920

Lee, S. H., Yang, J., Goddard, M. E., Visscher, P. M., & Wray, N. R. (2012). Estimation of pleiotropy between complex diseases using single-nucleotide polymorphism-derived genomic relationships and restricted maximum likelihood. *Bioinformatics*, *28*(19), 2540–2542. https://doi.org/10.1093/BIOINFORMATICS/BTS474

Li, H., Wang, C., Zhong, C., Su, A., Xiong, C., Wang, J., & Liu, J. (2017). Mapping Urban Bare Land Automatically from Landsat Imagery with a Simple Index. *Remote Sensing 2017, Vol. 9, Page 249*, *9*(3), 249. https://doi.org/10.3390/RS9030249

Li, K., Feng, M., Biswas, A., Su, H., Niu, Y., & Cao, J. (2020a). Driving Factors and Future Prediction of Land Use and Cover Change Based on Satellite Remote Sensing Data by the LCM Model: A Case Study from Gansu Province, China. *Sensors 2020, Vol. 20, Page 2757*, *20*(10), 2757. https://doi.org/10.3390/S20102757

Li, K., Feng, M., Biswas, A., Su, H., Niu, Y., & Cao, J. (2020b). Driving Factors and Future Prediction of Land Use and Cover Change Based on Satellite Remote Sensing Data by the LCM Model: A Case Study from Gansu Province, China. *Sensors 2020, Vol. 20, Page 2757*, *20*(10), 2757. https://doi.org/10.3390/S20102757

Mallick, J., Kant, Y., & Bharath, B. D. (2008). Estimation of land surface temperature over Delhi using Landsat-7 ETM+. *J. Ind. Geophys. Union*, *12*(3), 131–140.

NASAPOWER CERES. (2024). *POWER | Data Access Viewer*. https://power.larc.nasa.gov/data-access-viewer/

Nations, U. (n.d.). *Population | United Nations*. Retrieved May 31, 2024, from https://www.un.org/en/global-issues/population

Neteler, M. (2010). Estimating Daily Land Surface Temperatures in Mountainous Environments by Reconstructed MODIS LST Data. *Remote Sensing 2010, Vol. 2, Pages 333-351*, *2*(1), 333–351. https://doi.org/10.3390/RS1020333

Nichol, J. E., & To, P. H. (2012). Temporal characteristics of thermal satellite images for urban heat stress and heat island mapping. *ISPRS Journal of Photogrammetry and Remote Sensing*, *74*, 153–162. https://doi.org/10.1016/J.ISPRSJPRS.2012.09.007

Norman, J. M., & Becker, F. (1995a). Terminology in thermal infrared remote sensing of natural surfaces. *Agricultural and Forest Meteorology*, *77*(3–4), 153–166. https://doi.org/10.1016/0168-1923(95)02259-Z

Norman, J. M., & Becker, F. (1995b). Terminology in thermal infrared remote sensing of natural surfaces. *Agricultural and Forest Meteorology*, *77*(3–4), 153–166. https://doi.org/10.1016/0168-1923(95)02259-Z

Ogashawara, I., Da, V., & Brum Bastos, S. (2012). A Quantitative Approach for Analyzing the Relationship between Urban Heat Islands and Land Cover. *Remote Sensing 2012, Vol. 4, Pages 3596-3618*, *4*(11), 3596–3618. https://doi.org/10.3390/RS4113596

Oke, T. R., & Cleugh, H. A. (1987). Urban heat storage derived as energy balance residuals. *Boundary-Layer Meteorology*, *39*(3), 233–245. https://doi.org/10.1007/BF00116120/METRICS

Pal, S., & Ziaul, S. (2017). Detection of land use and land cover change and land surface temperature in English Bazar urban centre. *The Egyptian Journal of Remote Sensing and Space Science*, *20*(1), 125–145. https://doi.org/10.1016/J.EJRS.2016.11.003

Powell, S. L., Cohen, W. B., Yang, Z., Pierce, J. D., & Alberti, M. (2008). Quantification of impervious surface in the Snohomish Water Resources Inventory Area of Western Washington from 1972–2006. *Remote Sensing of Environment*, *112*(4), 1895–1908. https://doi.org/10.1016/J.RSE.2007.09.010

Qin, Z., & Karnieli, A. (1999). Progress in the remote sensing of land surface temperature and ground emissivity using NOAA-AVHRR data. *International Journal of Remote Sensing*, *20*(12), 2367–2393. https://doi.org/10.1080/014311699212074

Rasul, A., Balzter, H., Ibrahim, G. R. F., Hameed, H. M., Wheeler, J., Adamu, B., Ibrahim, S., & Najmaddin, P. M. (2018). Applying Built-Up and Bare-Soil Indices from Landsat 8 to Cities in Dry Climates. *Land 2018, Vol. 7, Page 81*, *7*(3), 81. https://doi.org/10.3390/LAND7030081

Rongali, G., Keshari, A. K., Gosain, A. K., & Khosa, R. (2018). Split-Window Algorithm for Retrieval of Land Surface Temperature Using Landsat 8 Thermal Infrared Data. *Journal of Geovisualization and Spatial Analysis*, *2*(2), 1–19. https://doi.org/10.1007/S41651-018-0021-Y/METRICS

Sheik Mujabar, P. (2019). Spatial-temporal variation of land surface temperature of Jubail Industrial City, Saudi Arabia due to seasonal effect by using Thermal Infrared Remote Sensor (TIRS) satellite data. *Journal of African Earth Sciences*, *155*, 54–63. https://doi.org/10.1016/J.JAFREARSCI.2019.03.008

Sobrino, J. A., Jiménez-Muñoz, J. C., & Paolini, L. (2004). Land surface temperature retrieval from LANDSAT TM 5. *Remote Sensing of Environment*, *90*(4), 434–440. https://doi.org/10.1016/J.RSE.2004.02.003

Streutker, D. R. (2002). A remote sensing study of the urban heat island of Houston, Texas. *International Journal of Remote Sensing*, *23*(13), 2595–2608. https://doi.org/10.1080/01431160110115023

Sun, Z., Wang, C., Guo, H., & Shang, R. (2017). A Modified Normalized Difference Impervious Surface Index (MNDISI) for Automatic Urban Mapping from Landsat Imagery. *Remote Sensing 2017, Vol. 9, Page 942*, *9*(9), 942. https://doi.org/10.3390/RS9090942

Ullah, S., Ahmad, K., Sajjad, R. U., Abbasi, A. M., Nazeer, A., & Tahir, A. A. (2019). Analysis and simulation of land cover changes and their impacts on land surface temperature in a lower Himalayan region. *Journal of Environmental Management*, *245*, 348–357. https://doi.org/10.1016/j.jenvman.2019.05.063

Voogt, J. A., & Oke, T. R. (2003). Thermal remote sensing of urban climates. *Remote Sensing of Environment*, *86*(3), 370–384. https://doi.org/10.1016/S0034-4257(03)00079-8

Xu, H. (2010). Analysis of Impervious Surface and its Impact on Urban Heat Environment using the Normalized Difference Impervious Surface Index (NDISI). *Photogrammetric Engineering and Remote Sensing*, *76*(5), 557–565. https://doi.org/10.14358/PERS.76.5.557

Yang, C., He, X., Yan, F., Yu, L., Bu, K., Yang, J., Chang, L., & Zhang, S. (2017). Mapping the influence of land use/land cover changes on the urban heat island effect-A case study of Changchun, China. *Sustainability (Switzerland)*, *9*(2). https://doi.org/10.3390/SU9020312

Yeneneh, N., Elias, E., & Feyisa, G. L. (2022). Detection of land use/land cover and land surface temperature change in the Suha Watershed, North-Western highlands of Ethiopia. *Environmental Challenges*, *7*, 100523. https://doi.org/10.1016/J.ENVC.2022.100523